SCIENTIFIC REPORTS

OPEN

Dependences of microstructure on electromagnetic interference shielding properties of nano-layered Ti_3AlC_2 ceramics

Received: 15 September 2017
Accepted: 2 May 2018
Published online: 21 May 2018

Yongqiang Tan, Heng Luo, Xiaosong Zhou, Shuming Peng & Haibin Zhang

The microstructure dependent electromagnetic interference (EMI) shielding properties of nano-layered Ti_3AlC_2 ceramics were presented in this study by comparing the shielding properties of various Ti_3AlC_2 ceramics with distinct microstructures. Results indicate that Ti_3AlC_2 ceramics with dense microstructure and coarse grains are more favourable for superior EMI shielding efficiency. High EMI shielding effectiveness over 40 dB at the whole Ku-band frequency range was achieved in Ti_3AlC_2 ceramics by microstructure optimization, and the high shielding effectiveness were well maintained up to 600 °C. A further investigation reveals that only the absorption loss displays variations upon modifying microstructure by allowing more extensive multiple reflections in coarse layered grains. Moreover, the absorption loss of Ti_3AlC_2 was found to be much higher than those of highly conductive TiC ceramics without layered structure. These results demonstrate that nano-layered MAX phase ceramics are promising candidates of high-temperature structural EMI shielding materials and provide insightful suggestions for achieving high EMI shielding efficiency in other ceramic-based shielding materials.

Electromagnetic interference (EMI), which could cause detrimental effects on the performance of electronic devices, has drawn growing attentions with the repaid development of highly sensitive circuits[1,2]. Ceramic-based EMI shielding materials have been identified as novel electromagnetic shielding options in the past few years owning to their promising applications as light-weight structural EMI shielding components in areas of aircraft and aerospace[3–6]. Compared to traditional metal- and carbon-based EMI shielding materials, ceramic composites exhibit the great advantage of being mechanically stiff and thermo-stable, which could guarantee their functionality at harsh environments[6]. Besides, the relatively high permittivity and dielectric loss of ceramics are favourable for the attenuation of EMI waves[4,5,7–9]. Nevertheless, the commonly inferior electrical conductivity becomes a major obstacle to obtain high EMI shielding effectiveness (SE) in ceramics. Although the electrical conductivity and EMI SE of ceramics could be both significantly enhanced by incorporating highly conductive carbon materials such as carbon nanotubes (CNTs)[4,10], carbon fibers (C_f)[6,11], graphene nanoplatelets (GNPs)[5,7,8,12], and pyrolytic carbon[13,14], the incorporation of those carbon nanostructures in ceramic composites is hindered by the difficulty of homogenous dispersion and their poor oxidation resistance at high temperatures. Accordingly, it is of great interest to explore intrinsically conductive ceramics as effective high-temperature EMI shielding materials.

MAX phase ceramics which represent a class of layered ternary transition-metal carbides and nitrides with a general formula of $M_{n+1}AX_n$ (wherein M is an early transition metal, A is an A-group element, X is either C or N, and n varies from 1 to 3)[15] are ideal candidates of high-temperature structural EMI shielding materials owning to their satisfactory mechanical properties, intrinsically superior electrical conductivity and the nano-layered structure[15,16]. Ti_3AlC_2 and Ti_3SiC_2 are two most studied MAX phases and both have been reported to exhibit high EMI SE[17,18]. Preliminary investigation demonstrates that the nano-layered structure of MAX phases made a considerable contribution to the total shielding effectiveness[17].

As was well known, the physical properties of composites usually show remarkable variations upon the change of their microstructures such as porosity, average grain size and interfaces[2,19–22]. The physical properties of ceramics could be possibly enhanced by a large scale through the optimization of microstructures. Especially for highly

Innovation Research Team for Advanced Ceramics, Institute of Nuclear Physics and Chemistry, China Academy of Engineering Physics, Mianyang, 621900, China. Correspondence and requests for materials should be addressed to S.P. (email: pengshuming@caep.cn) or H.Z. (email: hbzhang@caep.cn)

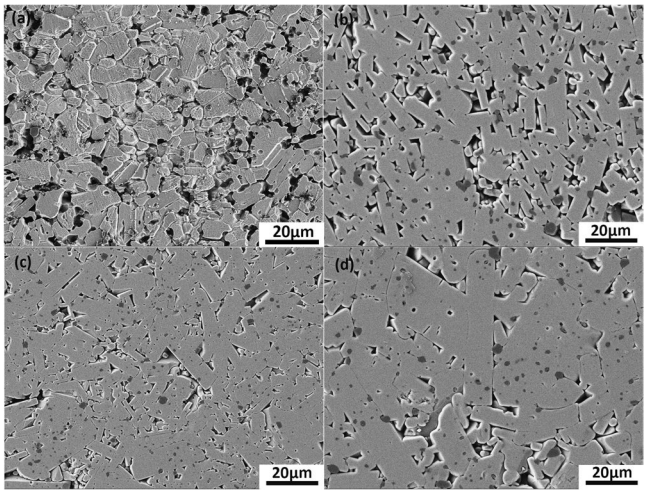

Figure 1. SEM images of polished surfaces of various Ti_3AlC_2 ceramics with distinct microstructures. (**a**) TAC-A; (**b**) TAC-B; (**c**) TAC-C; (**d**) TAC-D. All Ti_3AlC_2 ceramics show typical layered grains. The pressureless sintered sample shows certain degree of pores. With the increase of hot-pressing temperature, the microstructure becomes denser and shows significant grain growth.

Sample	Preparation Conditions	Relative Density	Electrical Conductivity
TAC-A	Pressureless sintering (1500 °C, 2 h)	91.2%	$2.4*10^6$ S/m
TAC-B	Hot-pressing (1350 °C, 15 min)	95.6%	$2.9*10^6$ S/m
TAC-C	Hot-pressing (1400 °C, 2 h)	98.5%	$3.0*10^6$ S/m
TAC-D	Hot-pressing (1400 °C,2 h) + Pressureless sintering (1500 °C, 10 h)	98.2%	$3.2*10^6$ S/m
TiC-A	Hot-pressing (1800 °C, 15 min)	98.6%	$4.2*10^6$ S/m
TiC-B	Hot-pressing (1950 °C, 2 h)	98.9%	$4.7*10^6$ S/m

Table 1. Comparison of relative density and electrical conductivity of various Ti_3AlC_2 and TiC ceramics.

conductive nano-layered structures, the grain size, aspect ratios and the alignment are supposed to have a decisive influence on the EMI shielding properties[20]. For example, significantly enhanced shielding efficiency was recently reported in highly aligned graphene/polymer nanocomposites[20]. However, no studies on the dependences of microstructures on EMI shielding properties of ceramics have been reported to our best knowledge. Accordingly, it is of great interest to study the effects of microstructure on the EMI shielding properties not only to obtain excellent high-temperature EMI shielding properties in MAX phase ceramics but also to unfold the origin of high EMI SE in ceramics with unique microstructure. Compared to Ti_3SiC_2, Ti_3AlC_2 exhibits much better oxidation resistance at high temperatures[23] and is therefore more suitable for high-temperature applications. Accordingly, Ti_3AlC_2 was chosen as study object, and four typical types of nano-layered Ti_3AlC_2 ceramics with different microstructures were fabricated by pressureless and hot-press sintering as well as their combination. As a comparison, the EMI shielding properties of highly conductive TiC ceramics without nano-layered structure were also examined. The influences of microstructure on the high-temperature EMI shielding properties were investigated systematically, and the mechanisms for high EMI SE in Ti_3AlC_2 ceramics were presented.

Results and Discussion

Figure 1 exhibits the SEM images of polished and etched surfaces of the various Ti_3AlC_2 ceramics prepared by different methods (given in Table 1). Obviously, all Ti_3AlC_2 ceramics exhibit distinct microstructures. The pressureless-sintered sample shows certain amounts of pores, which is consistent with its relatively lower relative density around 91% as indicated in Table 1. Besides, the aspect ratio of pressureless-sintered Ti_3AlC_2 grains is relatively low due to the absence of pressure during sintering. All hot-pressed Ti_3AlC_2 ceramics exhibit dense microstructures and layered grains with higher aspect ratios. The distributions of grain level dimension for different Ti_3AlC_2 ceramics were statistically calculated and exhibited in Fig. S1. The majority of grains for pressureless-sintered Ti_3AlC_2 ceramic (TAC-A) show level dimensions in the range of 8–14 μm. The average level dimension of hot-pressed samples increases significantly with increasing sintering temperature and duration, which is consistent with previous study[24]. Both the Ti_3AlC_2 ceramics sintered at 1350 °C for 15 min (TAC-B) and 1400 °C for 2 h (TAC-C) show broad level dimension distributions. The TAC-B shows a level dimension peak around 10 μm while the distribution peak of TAC-C locates at a higher size range around 20 μm. A followed thermal process at 1500 °C for 10 h further promotes the grain growth with a dominant percentage of grains with level dimension larger than 25 μm and a considerable percentage of grains with level dimension larger than 40 μm. All

the Ti_3AlC_2 ceramics exhibit the same single-phase crystal structure without detectable second phases, which can be evidenced by the XRD patterns shown in Fig. S2 in the supporting information.

The total SE (SE_T) of EMI shielding materials can be characterized as follows[25]:

$$SE_T = 10\log(P_i/P_t) = SE_R + SE_A + SE_M \quad (1)$$

in which SE_T, SE_A SE_R and SE_M denote the total SE, SE due to reflection, absorption loss and multiple reflections, respectively. SE_T, SE_R and SE_A were calculated from the *S*-parameters as follows[26],

$$SE_T = -\ 10\log\ |S_{12}|^2 \quad (2)$$

$$SE_R = -\ 10\log(1 - |S_{11}|^2) \quad (3)$$

$$SE_A = -\ 10\log(\frac{|S_{21}|^2}{1 - |S_{11}|^2}) \quad (4)$$

Figure 2a–c compare the frequency dependences of room-temperature SE_T, SE_R and SE_A respectively of Ti_3AlC_2 ceramics with different microstructures. The SE_T exhibits notable differences among various Ti_3AlC_2 ceramics. The pressureless sintered Ti_3AlC_2 ceramic exhibits the lowest SE_T around 30 dB, which is comparable to those of most ceramic-based composites[5,11,27]. The hot-pressed Ti_3AlC_2 ceramics exhibit remarkably enhanced SE_T compared to pressureless sintered sample. Further, the room-temperature SE_T of hot-pressed samples increases monotonically with the increase of grain size. TAC-D ceramic with the largest grain size shows the highest SE_T over 40 dB at the whole Ku-band, which means over 99.99% of the incident radiation could be effectively blocked with only 0.01% transmission. The room-temperature EMI SE_T of TAC-D ceramic is higher than most ceramic-based EMI shielding composites containing conductive particles or carbon nano-fillers[3–6,8,27], while the preparation of Ti_3AlC_2 ceramics is much less complicated. Moreover, the high SE_T of TAC-D ceramic is almost independent of the frequency. In Equation (1), the SE_A can be regarded as the energy dissipation of the electromagnetic microwave in the absorber and therefore the multiple reflection SE_M in single phase Ti_3AlC_2 ceramics actually is included in absorption because the re-reflected waves could get absorbed or dissipated within the material[1]. Accordingly, the SE_T could be expressed as,

$$SE_T = SE_R + SE_A \quad (5)$$

In order to have a deeper understanding on the origin of microstructure-dependent EMI shielding properties in Ti_3AlC_2 ceramics, the dependences of microstructure on the reflection loss SE_R and absorption loss SE_A of Ti_3AlC_2 ceramics were investigated and the results were exhibited in Fig. 3b and c respectively. It can be seen that the SE_R of Ti_3AlC_2 ceramics is almost independent of their microstructure. All Ti_3AlC_2 ceramics with various microstructures show similar SE_R values between 10 and 14 dB, especially, the SE_R of all the hot-pressed ceramics exhibit almost the same values at the whole Ku-band frequency range. The reflection loss of EMI shielding materials arises mainly from the impedance mismatch between the sample and the free space[25]. The extremely high electrical conductivity (~10^6 S/m) of Ti_3AlC_2 ceramics could lead to a huge impedance mismatch and therefore give rise to a high reflection loss. The pressureless sintered Ti_3AlC_2 ceramics exhibit inferior electrical conductivity due to high porosity (Table 1), accordingly, its SE_R is relatively lower. While for dense Ti_3AlC_2 ceramics, the influence of grain size on the conductivity is negligible and therefore the SE_R becomes almost independent of the microstructure. All Ti_3AlC_2 ceramics exhibit high absorption loss SE_A (Fig. 2c) which is much larger than SE_R, indicating that Ti_3AlC_2 ceramics are typically absorption-dominant EMI shielding materials. Specially, high SE_A of 30 dB which is almost 3 times larger than SE_R was obtained for TAC-D ceramic at 12.4 GHz. Being different from SE_R, the absorption loss shows obvious grain size dependence and becomes the major contribution to the variation of SE_T among Ti_3AlC_2 ceramics with different microstructures, as demonstrated in Fig. 2c. Hot-pressed Ti_3AlC_2 ceramics exhibit higher SE_A than pressureless sintered sample. For hot-pressed Ti_3AlC_2 ceramics, the SE_A increases gradually with increasing grain size. Therefore, it can be concluded that dense and coarse-grained microstructure with higher aspect ratios is more favorable for high EMI attenuation and the total EMI shielding in nano-layered Ti_3AlC_2 ceramics.

In order to further validate the significant contribution of the nano-layered structure to the absorption loss, the EMI shielding properties of highly conductive TiC ceramics without nano-layered structures were characterized and compared with those of Ti_3AlC_2 ceramics. Figure S3 shows the fracture surfaces of TiC ceramics sintered at different temperatures. Both TiC ceramics exhibit different microstructures from Ti_3AlC_2 ceramics without layered structures. It is apparent that the grain size of TiC-B is much larger than that of TiC-A. The frequency dependences of the EMI SE for different TiC ceramics were shown in Fig. 3. It is interesting to notice that, being different to that of Ti_3AlC_2 ceramics, the change of grain size did not bring significant variation of SE_T for TiC ceramics. Especially, the SE_A for fine- and coarse-grained TiC ceramics are almost the same. Compared to Ti_3AlC_2 ceramics, the TiC ceramics shows much lower SE_A while higher SE_R. The microstructure-independent SE_A of TiC ceramics varies in the range of 18–25 dB at the whole frequency range. The SE_R has almost equal contribution to the total shielding for both TiC ceramics. The different shielding properties between Ti_3AlC_2 and TiC further confirms that the nano-layered structure is responsible for the superior and microstructure-dependent SE_A in Ti_3AlC_2 ceramics. The reflection loss of Ti_3AlC_2 ceramics is considerably lower than that of TiC ceramics although both ceramics exhibit similar electrical conductivity as demonstrated in Table 1.

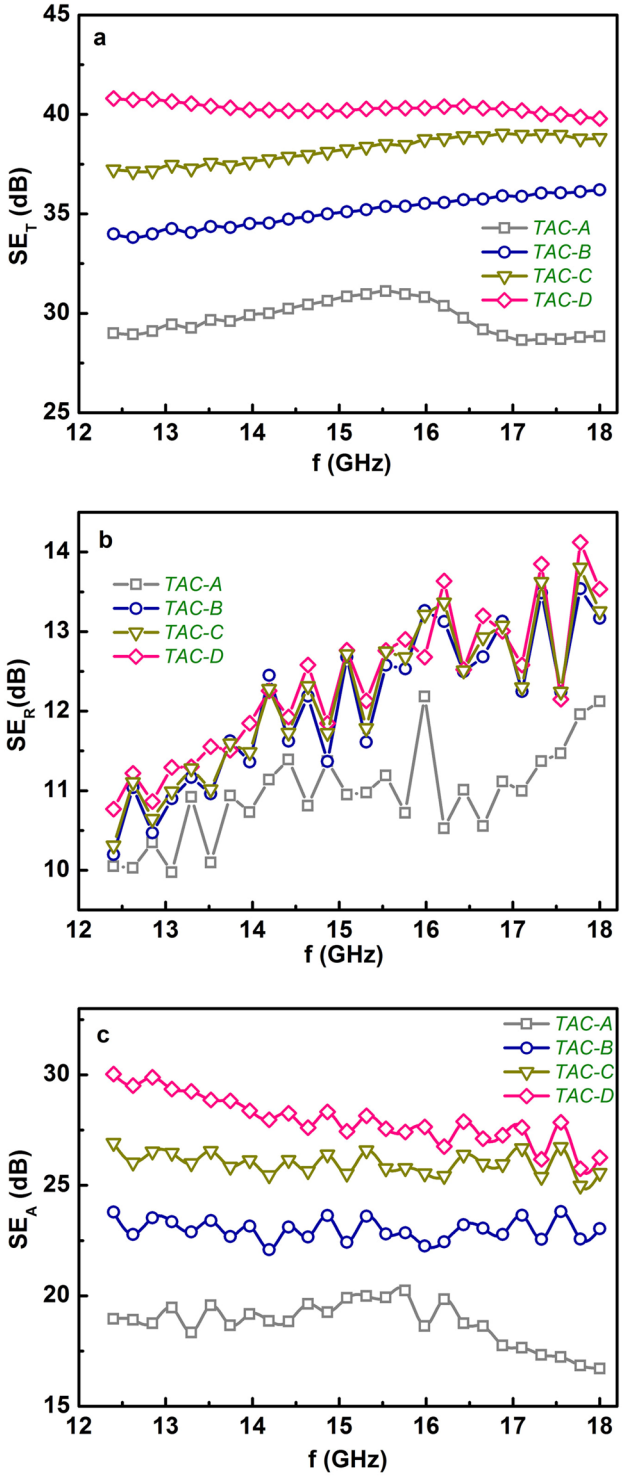

Figure 2. The frequency dependences of (**a**) the total shielding effectiveness SE_T, (**b**) reflection loss SE_R and (**c**) absorption loss SE_A of various Ti_3AlC_2 ceramics with distinct microstructures measured at room-temperature. Ti_3AlC_2 ceramics with various microstructures exhibit different EMI shielding capability and those differences mainly arose from the distinct absorption loss.

Similar to most EMI shielding materials with two-dimensional nano-layered structures, the high SE_A of nano-layered Ti_3AlC_2 ceramics arises mainly from two major attenuation mechanisms: the high electrical/dielectric loss and layered architecture[1,5,19,20,22]. Figure 4 presents the real (ε') and imaginary (ε'') parts of permittivity as well as the dielectric loss tan defined as[9]

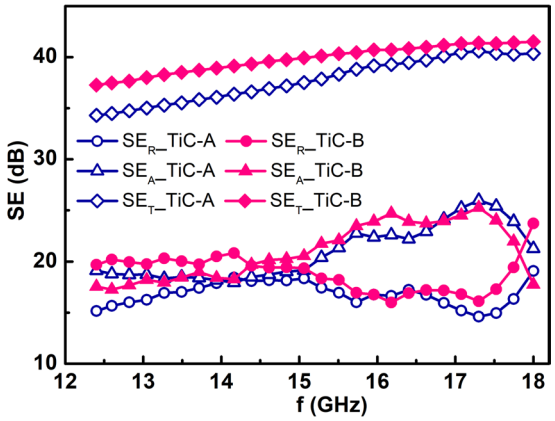

Figure 3. Comparison of the shielding effectiveness of TiC ceramics with different grain size. The shielding effectiveness was measured at room temperature. The shielding capability of TiC ceramics shows much weaker grain size dependence compared to Ti_3AlC_2 ceramics.

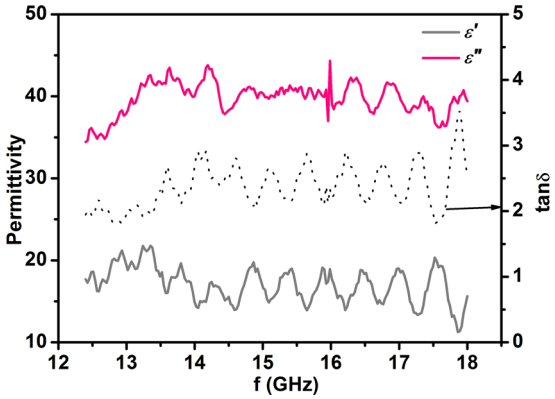

Figure 4. The frequency dependent permittivity (real part ε' and imaginary part ε'') and loss tangent ($\tan\delta = \varepsilon''/\varepsilon'$) of TAC-D ceramic measured at room-temperature. The Ti_3AlC_2 ceramics show high imaginary permittivity ε'' and high dielectric loss at the whole Ku band.

$$tan\delta = \varepsilon''/\varepsilon' \tag{6}$$

of TAC-D ceramic measured at room-temperature. It can be seen that Ti_3AlC_2 ceramics exhibit moderate real permittivity around 15 while significantly higher imaginary part of ~40. Consequently, the dielectric loss of Ti_3AlC_2 ceramics reaches a considerably high value around 2.5. The high electrical/dielectric loss of Ti_3AlC_2 ceramics arises from the abundant free electrons and a large quantity of unpaired defects[16]. The conduction current owing to the skin effect as well as the eddy current will contribute to the ohmic loss, and the unpaired defects will contribute to the dielectric loss. Compared to the electrical/dielectric loss, the multiple reflections also played a significant role in achieving high SE_A in nano-layered structures such as graphene and MAX phases, and the multiple reflections are more likely to display microstructure dependences in ceramics. Ti_3AlC_2 ceramics exhibit layered grains and therefore abundant flat grain boundaries. When the incident EMI radiations encounter those flat grain boundaries, a portion of the EMI radiations gets immediately reflected due to the impedance mismatch of adjacent layers with the others penetrating through these interfaces. The penetrated EMI radiations can be reflected back and forth between the adjacent grain boundaries. These multiple reflections could increase the length of EMI transmission pathway by a large scale and enhance the attenuation of EMI accordingly[1,7,8,20]. In coarse grains with high aspect ratios, a higher degree of multiple reflections can be expected due to the large surface area of a single grain boundary and thereby a higher absorption loss. Consequently, the origin of microstructure dependent EMI shielding effectiveness can be ascribed to the enhanced degree of multiple reflections with increasing level dimensions of layered Ti_3AlC_2 grains.

Figure 5 shows the frequency dependences of SE_T at different temperatures up to 600 °C for different Ti_3AlC_2 ceramics. It can be seen that the SE_T of all Ti_3AlC_2 ceramics only shows a slight decrease with increasing temperature. The variations of SE_T from room-temperature to 600 °C for all Ti_3AlC_2 ceramics is less than 10%. A high SE_T around 38 dB was still maintained at 600 °C for TAC-D ceramic, demonstrating that the EMI shielding properties of Ti_3AlC_2 ceramics have excellent thermo-stability and is well suitable for high-temperature EMI shielding applications. Figure S4 shows the frequency dependences of SE_R and SE_A of different Ti_3AlC_2 ceramics measured at

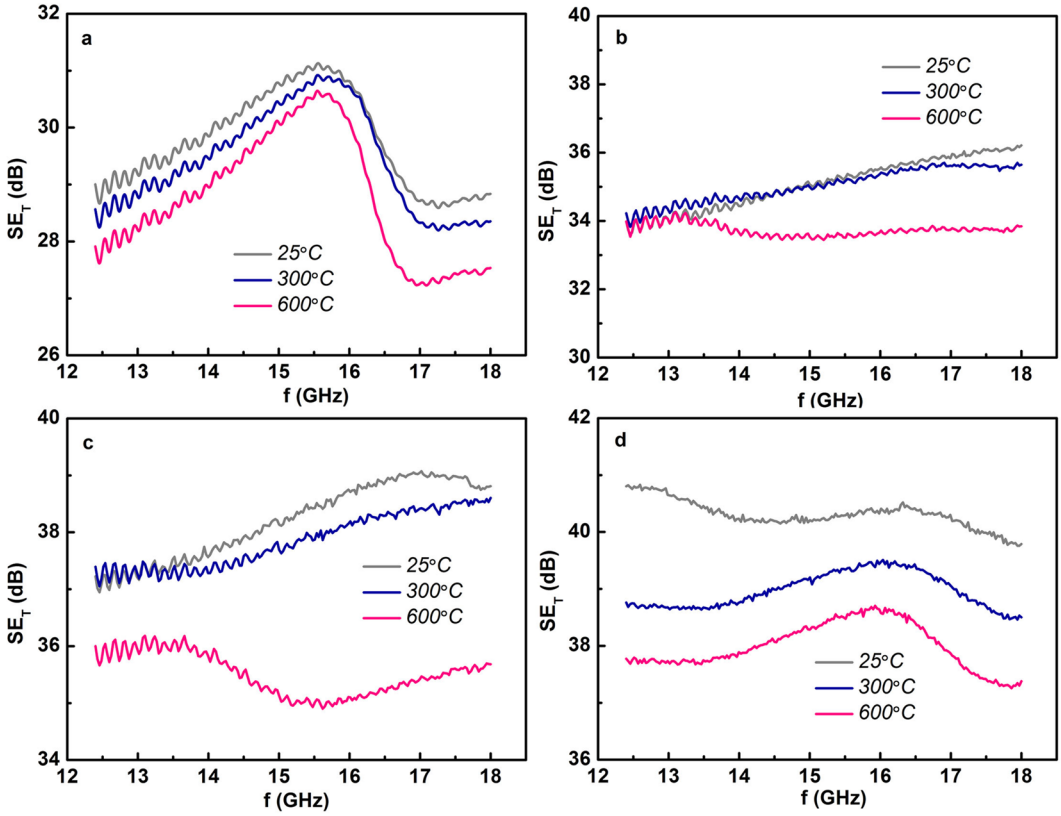

Figure 5. The frequency dependent SE_T of various Ti_3AlC_2 ceramics measured at different temperatures. (**a**). TAC-A; (**b**). TAC-B; (**c**). TAC-C; (**d**). TAC-D. The shielding effectiveness of all Ti_3AlC_2 ceramics exhibit satisfactory temperature stability and high EMI SE still persist at high temperatures.

600 °C. By comparing Fig. 2 and Fig. S4, it can be easily observed that for all Ti_3AlC_2 ceramics the SE_R kept almost the same with increasing temperature to 600 °C. Although the electrical conductivity of Ti_3AlC_2 ceramics tend to decrease with increasing temperature, the giant impedance mismatch between Ti_3AlC_2 ceramics and the air made the SE_A almost unaffected by the slight decrease of electrical conductivity. The decrease of SE_T solely arises from the decrease of SE_A with increasing temperature. The SE_A decrease equally for all Ti_3AlC_2 ceramics and TAC-D ceramic still exhibits the highest SE_A around 26 dB in the Ku-band frequency range at 600 °C. The slight decrease of absorption loss with increasing temperature can be ascribed to the less internal friction of dipole reorientation at high temperatures.

Conclusions

Various Ti_3AlC_2 ceramics with distinct microstructures were prepared by pressureless sintering and hot-pressing. Their EMI shielding properties were characterized at Ku-band frequency range from room temperature to 600 °C. It was found that the EMI shielding properties of Ti_3AlC_2 ceramics display remarkable microstructure dependences. High EMI shielding effectiveness over 40 dB was obtained in coarse-grained Ti_3AlC_2 ceramic and the excellent shielding properties were well maintained at high temperatures up to 600 °C. The variations of EMI SE_T with changing microstructure dominantly arises from the variation of absorption loss SE_A which is related to the high electric/dielectric loss and more importantly the nano-layered structure of Ti_3AlC_2. Coarse Ti_3AlC_2 grains with high aspect ratio are more favourable for high multiple reflections of EMI waves and consequently more absorption loss. Highly conductive TiC ceramics without nano-layered structure exhibit almost microstructure-independent shielding properties and much lower absorption loss than that of Ti_3AlC_2 ceramics. These results indicate that Ti_3AlC_2 ceramic are promising high-temperature EMI shielding materials.

Methods

Ti_3AlC_2 powder (purity $\geq$ 98%, ~300 mesh) was purchased from Forsman (Beijing) Scientific Co., Ltd. Four types of Ti_3AlC_2 ceramics referred as TAC-A, TAC-B, TAC-C and TAC-D respectively were prepared by different sintering techniques at different temperatures. In the case of TAC-A, the Ti_3AlC_2 powder was first cold-pressed into pellets of 50 mm in diameter and 2 mm in thickness under a uniaxial pressure of 50 MPa, and then pressureless-sintered in Ar atmosphere at 1450 °C for 120 min; In the case of TAC-B, TAC-C and TAC-D, the Ti_3AlC_2 powder was placed in a 50 mm diameter graphite die and hot-pressed in Ar atmosphere under different conditions: TAC-B was hot-pressed at 1350 °C for 15 min; TAC-C was hot-pressed at 1400 °C for 120 min; TAC-D was hot-pressed at 1400 °C for 120 min followed by a pressureless sintering in Ar atmosphere at 1450 °C for 500 min. During the hot-press sintering a uniaxial pressure of 30 MPa was applied. Two distinct types of TiC

ceramics with 50 mm in diameter and 2 mm in thickness were prepared by hot-pressing at 1800 °C for 15 min (TiC-A) and 1950 °C for 2 h (TiC-B) respectively using commercial TiC powders (~100 nm, Forsman (Beijing) Scientific Co., Ltd.). A uniaxial pressure of 60 MPa was applied during sintering. The bulk density of the prepared ceramics was measured using the Archimedes' method. Crystalline phases were characterized by X-ray diffraction (XRD). For microstructure characterization, the Ti_3AlC_2 samples were polished using SiC papers and diamond suspensions down to 0.5 μm. The well-polished surfaces were further etched in an acid solution with a volume ratio of HF: HNO_3:H_2O = 1:1:3 for 45 s. The morphology of different specimens was observed by field emission scanning electron microscopy (FE-SEM). The grain size distribution of Ti_3AlC_2 ceramics was analysed on SEM images (with a magnification of 1000×) of polished and etched surfaces using ImageJ software. In order to ensure the accuracy of measurement, at least 1000 grains from the polished and etched surfaces were considered to statistically obtain the grain level dimension distributions.

For EMI SE characterization, specimens with dimensions of 22.86 mm × 10.16 mm × 1.00 mm were cut and polished. The magnitudes of complex scattering parameters (S-parameters) that correspond to reflection (S_{11} or S_{22}) and transmission (S_{21} or S_{12}) in the frequency range of 12.4~18 GHz (Ku band) were determined through wave-guide method using a vector network analyzer (Agilent N5230A). For accuracy of measurement, the device is carefully calibrated with Through-Reflect-Line (TRL) approach. The high-temperature measurement of SE was performed in a waveguide heated by an inner heater at a rate of 10 °C/min. The temperature range is 25–600 °C and each temperature spot was stabilized for 10 min in order to ensure the accuracy of measurement.

References

1. Shahzad, F. *et al*. Electromagnetic interference shielding with 2D transition metal carbides (MXenes). *Science* **353**, 1137–1140 (2016).
2. Chen, Z., Xu, C., Ma, C., Ren, W. & Cheng, H. Lightweight and flexible graphene foam composites for high-performance electromagnetic interference shielding. *Adv. Mater.* **25**, 1296–1300 (2013).
3. Mu, Y. *et al*. High-temperature dielectric and electromagnetic interference shielding properties of SiC_f/SiC composites using Ti_3SiC_2 as inert filler. *Compos. A* **77**, 195–203 (2015).
4. Qing, Y. *et al*. Multiwalled carbon nanotubes–$BaTiO_3$/silica composites with high complex permittivity and improved electromagnetic interference shielding at elevated temperature. *J. Eur. Ceram. Soc.* **34**, 2229–2237 (2014).
5. Wen, B. *et al*. Reduced graphene oxides: light-weight and high-efficiency electromagnetic interference shielding at elevated temperatures. *Adv. Mater.* **26**, 3484–3489 (2014).
6. Chen, L. *et al*. Mechanical and electromagnetic shielding properties of carbon fiber reinforced silicon carbide matrix composites. *Carbon* **95**, 10–19 (2015).
7. Qing, Y., Wen, Q., Luo, F., Zhou, W. & Zhu, D. Graphene nanosheets/$BaTiO_3$ ceramics as highly efficient electromagnetic interference shielding materials in the X-band. *J. Mater. Chem. C* **4**, 371–375 (2016).
8. Qing, Y., Wen, Q., Luo, F. & Zhou, W. Temperature dependence of the electromagnetic properties of graphene nanosheet reinforced alumina ceramics in the X-band. *J. Mater. Chem. C* **4**, 4853–4862 (2016).
9. Song, W. *et al*. High dielectric loss and its monotonic dependence of conducting-dominated multiwalled carbon nanotubes/silica nanocomposite on temperature ranging from 373 to 873 K in X-band. *Appl. Phys. Lett.* **94**, 233110 (2009).
10. Wen, B. *et al*. Temperature dependent microwave attenuation behavior for carbon-nanotube/silica composites. *Carbon* **65**, 124–139 (2013).
11. Cao, M., Song, W., Hou, Z., Wen, B. & Yuan, J. The effects of temperature and frequency on the dielectric properties, electromagnetic interference shielding and microwave-absorption of short carbon fiber/silica composites. *Carbon* **48**, 788–796 (2010).
12. Cao, M., Wang, X., Cao, W. & Yuan, J. Ultrathin graphene: electrical properties and highly efficient electromagnetic interference shielding. *J. Mater. Chem. C* **3**, 6589–6599 (2015).
13. Li, X., Zhang, L. & Yin, X. Synthesis and electromagnetic shielding property of pyrolytic carbon-silicon nitride ceramics with dense silicon nitride coating. *J. Am. Ceram. Soc.* **95**, 1038–1041 (2012).
14. Li, X., Zhang, L. & Yin, X. Electromagnetic properties of pyrolytic carbon-Si_3N_4 ceramics with gradient PyC distribution. *J. Eur. Ceram. Soc.* **33**, 647–651 (2013).
15. Wang, J. & Zhou, Y. Recent progress in theoretical prediction, preparation, and characterization of layered ternary transition-metal carbides. *Annu. Rev. Mater. Res.* **39**, 415–443 (2009).
16. Zhou, Y. C., Wang, X. H., Sun, Z. M. & Chen, S. Q. Electronic and structural properties of the layered ternary carbide Ti_3AlC_2. *J. Mater. Chem.* **11**, 2335–2339 (2001).
17. Tan, Y., Luo, H., Zhang, H., Zhou, X. & Peng, S. High-temperature electromagnetic interference shielding of layered Ti_3AlC_2 ceramics. *Scripta Mater.* **134**, 47–51 (2017).
18. Shi, S., Zhang, L. & Li, J. Ti_3SiC_2 material: An application for electromagnetic interference shielding. *Appl. Phys. Lett.* **93**, 172903 (2008).
19. Yan, D. *et al*. Structured reduced graphene oxide/polymer composites for ultra-efficient electromagnetic interference shielding. *Adv. Funct. Mater.* **25**, 559–566 (2015).
20. Yousefi, N. *et al*. Highly aligned graphene/polymer nanocomposites with excellent dielectric properties for high-performance electromagnetic interference shielding. *Adv. Mater.* **26**, 5480–5487 (2014).
21. Yuan, B., Yu, L., Sheng, L., An, K. & Zhao, X. Comparison of electromagnetic interference shielding properties between single-wall carbon nanotube and graphene sheet/polyaniline composites. *J. Phys. D* **45**, 235108 (2012).
22. Han, M. *et al*. Ti_3C_2 MXenes with Modified Surface for High-Performance Electromagnetic Absorption and Shielding in the X-Band. *ACS Appl. Mater. Inter.* **8**, 21011–21019 (2016).
23. Wang, X. H. & Zhou, Y. C. Oxidation behavior of Ti_3AlC_2 at 1000–1400 °C in air. *Corros. Sci.* **45**, 891–907 (2003).
24. Wan, D. T. *et al*. Effect of grain size, notch width, and testing temperature on the fracture toughness of $Ti_3Si(Al)C_2$ and Ti_3AlC_2 using the chevron-notched beam (CNB) method. *J. Eur. Ceram. Soc.* **28**, 663–669 (2008).
25. Chung, D. D. L. Electromagnetic interference shielding effectiveness of carbon materials. *Carbon* **39**, 279–285 (2001).
26. Al-Saleh, M. H. & Sundararaj, U. Electromagnetic interference shielding mechanisms of CNT/polymer composites. *Carbon* **47**, 1738–1746 (2009).
27. Shi, S. & Ji, L. The effect of multi-wall carbon nanotubes on electromagnetic interference shielding of ceramic composites. *Nanotechnology* **19**, 255707 (2008).

Acknowledgements

This work was supported by the National Natural Science Foundation of China (Grants Nos 91326102 and 51532009), and the Science and Technology Development Foundation of China Academy of Engineering Physics (Grant No. 2013A0301012). H. Zhang is grateful to the foundation by the Recruitment Program of Global Youth Experts and the Youth Hundred Talents Project of Sichuan Province.

Author Contributions

Y.T. and H.Z. conceived the ideas. Y.T. prepared samples. H.L. conducted the characterizations. Y.T., X.Z., S.P. and H.Z. wrote the paper.

Additional Information

Supplementary information accompanies this paper at https://doi.org/10.1038/s41598-018-26256-0.

Competing Interests: The authors declare no competing interests.

Publisher's note: Springer Nature remains neutral with regard to jurisdictional claims in published maps and institutional affiliations.